ACS Chemical Neuroscience

Research Article

pubs.acs.org/chemneuro

Novel Trimodal MALDI Imaging Mass Spectrometry (IMS3) at 10 μm Reveals Spatial Lipid and Peptide Correlates Implicated in Aβ Plaque Pathology in Alzheimer's Disease

Ibrahim Kaya,[†] Dimitri Brinet,[†,‡] Wojciech Michno,[†] Mehmet Başkurt,[†,§] Henrik Zetterberg,[†,∥,⊥,#] Kaj Blenow,[†,∥] and Jörg Hanrieder*[,†,∥,⊥]

[†]Department of Psychiatry and Neurochemistry, Sahlgrenska Academy at the University of Gothenburg, Mölndal Hospital, House V3, 43180 Mölndal, Sweden

[‡]Department of Chemistry and Molecular Biology, University of Gothenburg, Kemivägen 10, 405 30 Gothenburg, Sweden

[§]Department of Chemistry, İzmir Institute of Technology, Urla 35430, İzmir, Turkey

[∥]Clinical Neurochemistry Laboratory, Sahlgrenska University Hospital Mölndal, House V3, 43180 Mölndal, Sweden

[⊥]Department of Molecular Neuroscience, Institute of Neurology, University College London, Queen Square, London WC1N 3BG, United Kingdom

[#]UK Dementia Research Institute, University College London, London WC1N 3AR, United Kingdom

Supporting Information

ABSTRACT: Multimodal chemical imaging using matrix-assisted laser desorption/ionization mass spectrometry (MALDI-MS) can provide comprehensive molecular information in situ within the same tissue sections. This is of relevance for studying different brain pathologies such as Alzheimer's disease (AD), where recent data suggest a critical relevance of colocalizing Aβ peptides and neuronal lipids. We here developed a novel trimodal, high-resolution (10 μm) MALDI imaging MS (IMS) paradigm for negative and positive ion mode lipid analysis and subsequent protein ion imaging on the same tissue section. Matrix sublimation of 1,5-diaminonaphthalene (1,5-DAN) enabled dual polarity lipid MALDI IMS on the same pixel points at high spatial resolutions (10 μm) and with high spectral quality. This was followed by 10 μm resolution protein imaging on the same measurement area, which allowed correlation of lipid signals with protein distribution patterns within distinct cerebellar regions in mouse brain. The demonstrated trimodal imaging strategy (IMS3) was further shown to be an efficient approach for simultaneously probing Aβ plaque-associated lipids and Aβ peptides within the hippocampus of 18 month-old transgenic AD mice (tgArcSwe). Here, IMS3 revealed a strong colocalization of distinct lipid species including ceramides, phosphatidylinositols, sulfatides (Cer 18:0, PI 38:4, ST 24:0) and lysophosphatidylcholines (LPC 16:0, LPC 18:0) with plaque-associated Aβ isoforms (Aβ 1−37, Aβ 1−38, Aβ 1−40). This highlights the potential of IMS3 as an alternative, superior approach to consecutively performed immuno-based Aβ staining strategies. Furthermore, the IMS3 workflow allowed for multimodal in situ MS/MS analysis of both lipids and Aβ peptides. Altogether, the here presented IMS3 approach shows great potential for comprehensive, high-resolution molecular analysis of histological features at cellular length scales with high chemical specificity. It therefore represents a powerful approach for probing the complex molecular pathology of, e.g., neurodegenerative diseases that are characterized by neurotoxic protein aggregation.

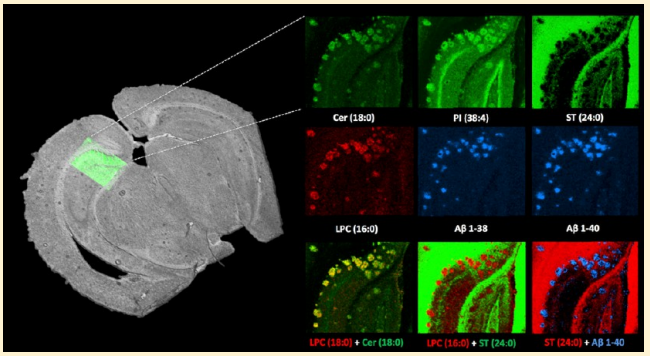

KEYWORDS: *MALDI imaging mass spectrometry, trimodal MALDI imaging MS, Alzheimer's disease, plaque pathology, neuronal lipids, Aβ peptides*

INTRODUCTION

Matrix-assisted laser desorption/ionization based imaging mass spectrometry (MALDI-IMS) is a rapidly developing technique for spatial profiling of endogenous biochemical species in situ including metabolites,[1] peptides,[2] proteins,[2,3] and lipids.[4,5] The suitability of MALDI-IMS for comprehensive, unlabeled, spatial analysis for a wide range of chemical species in situ makes it a powerful technique to probe the molecular histopathology in complex biological tissues, such as brain tissue.[6] Although MALDI-IMS has been successfully applied for a variety of

Received: August 14, 2017
Accepted: September 19, 2017
Published: September 19, 2017

DOI: 10.1021/acschemneuro.7b00314
ACS Chem. Neurosci. 2017, 8, 2778−2790

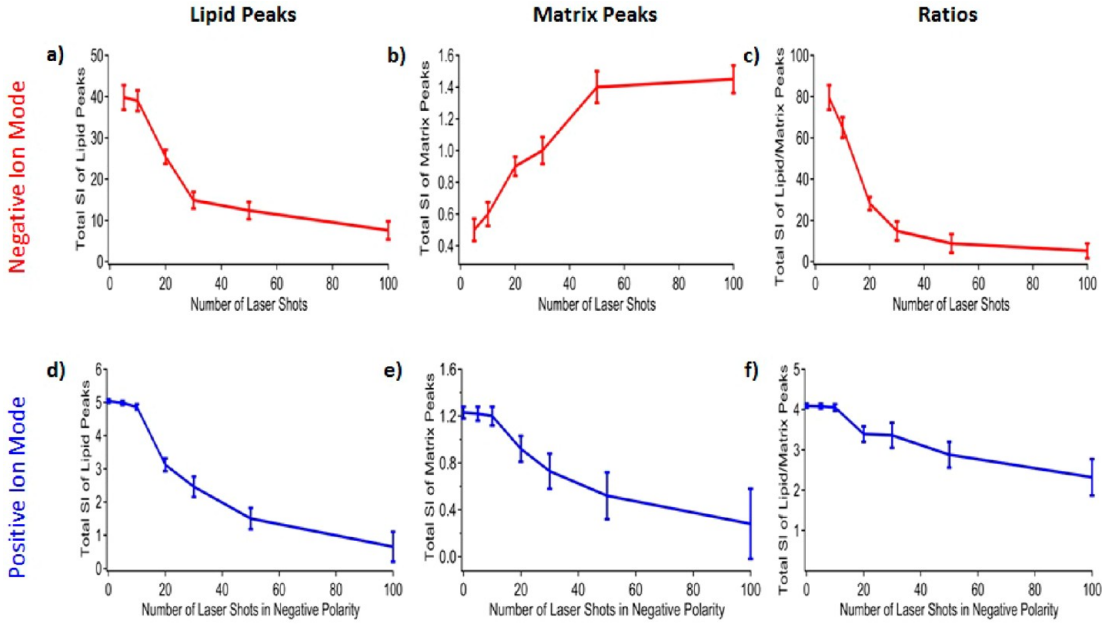

Figure 1. Effect of number of laser shots (5, 10, 20, 30, 50, 100) on (a) total signal intensity of lipid peaks in negative ion mode (300−2000 Da, excluding matrix peaks) and (b) total signal intensity of matrix-derived peaks (300−650 Da) acquired on cerebellar areas equivalent in size (80 pixel points) and morphology. (c) The ratio of the total signal intensity of lipid peaks to total signal intensity of matrix derived peaks in negative ion mode (red) (d−f). Positive ion signals (blue) following negative ion mode imaging experiments on the same pixel point. (d) Total signal intensity of lipid peaks and (e) matrix-derived peaks in positive polarity along with the ratio of the total signal intensity lipid peaks to matrix-derived peaks (f) obtained by subsequent imaging in positive ion mode on the same pixel points. Zero shots (positive polarity) data were obtained from an equivalent nonirradiated area using a constant number of laser shots (50). Error bars: SD (n = 5).

biomedical analysis,[7−9] the fundamental factors affecting selectivity, ionization efficiency, sensitivity, mass resolution, and reproducibility are still not fully understood.[10−12] This is due to the complexity of the ionization process and the interaction of the laser with the matrix compound, competing charge generation and transfer processes in laser desorption plumes, as well as different physicochemical properties of the matrix and analyte molecules.[9−11,13−15] Therefore, the choice of the matrix compound and matrix application strategy are important factors as all matrix compounds have varying restrictions with respect to analyte selectivity (e.g., lipids, proteins), analyte polarity, crystal size, and optimal matrix application conditions.[6] In order to perform comprehensive imaging of lipids, peptides, and proteins, typically multiple analyses on consecutive tissue sections are required per biological sample using different matrix preparation approaches. However, in these cases, the correlation of molecular histopathology is challenging, as anatomical features can vary from one tissue section to another, if their size is not exceeding the thickness of the tissue section. With respect to the diversity in biomolecular histopathology associated with different diseases, it is therefore desired to correlate molecular information with histological features on the same tissue section.

So far, only few studies have demonstrated subsequent MALDI-IMS analysis on a single tissue section.[5,6,16−19] For example, multiple MALDI-IMS analyses were demonstrated for single rat brain tissue sections by recoating the tissue after the loss of matrix molecules. This allowed repeat lipid imaging at >100 μm spatial resolution along with multiple MS/MS experiments on a single tissue section.[16] Furthermore, successful application of dual polarity imaging of phospholipids within a single mouse brain section was described with a spatial resolution of 100 μm using a 50 μm offset in between the two modalities.[5]

In the present study, we developed a three step, multimodal MALDI-IMS paradigm (IMS3), for comprehensive imaging of neuronal lipids and proteins at high spatial resolution (10 μm) on the same mouse brain section. Here, we used a histology-compatible MALDI-IMS approach[20] based on sublimation of a low-ionization energy matrix, 1,5-diaminonaphthalene (1,5-DAN),[5] facilitating subsequent, dual polarity lipid imaging in positive- and negative-ion mode on the same pixel points. This was followed by temperature-controlled spraying of 2,5-dihydroxy-acetophenone (2,5-DHA) matrix for subsequent protein imaging, which allowed acquisition and correlation of lipid and protein/peptide imaging data within specific brain regions on the same mouse brain tissue section. The optimized, trimodal imaging MS workflow was then applied to probe amyloid-β plaque-associated lipids and Aβ peptide isoforms in a transgenic mouse model (tgArcSwe) of Alzheimer's disease.

RESULTS AND DISCUSSION

High-Resolution (10 μm), Dual Polarity Lipid MALDI-IMS on the Same Pixel Points. For sensitive and reproducible MALDI-IMS analysis at high spatial resolution, the choice of matrix compound and matrix application technique are the key factors.[5] Most wet matrix deposition techniques can lead to lateral analyte diffusion, which impacts spatial resolution.[21] High laser fluence, as required for certain MALDI matrices, can furthermore cause extensive matrix cluster formation,[13,20] in-source fragmentation,[13] as well as impact the molecular tissue morphology, all resulting in analyte delocalization and tissue distortion.[20] Therefore, it is important to choose a sensitive matrix compound for the respective target analytes in conjunction with a compatible matrix application

DOI: 10.1021/acschemneuro.7b00314
ACS Chem. Neurosci. 2017, 8, 2778−2790

protocol to obtain spatially well-resolved, intense ion signals while preserving the tissue morphology.[20]

Here, we investigated high-spatial resolution (10 μm) dual polarity MALDI imaging mass spectrometry of lipids within the mouse cerebellum using an approach based on sublimation of 1,5-DAN for matrix deposition.[5] Despite the high abundance of lipids and their efficient ionization behavior in MALDI, the structural diversity of lipids and the complexity of the laser desorption/ionization process limit comprehensive lipid profiling within a single IMS analysis. For example, sphingomyelins (SM), phosphatidylcholines (PC), and neutral lipids such as triacylglycerols (TG) and cerebrosides (Crb) are usually observed in positive ion mode, whereas other phospholipids, including phosphatidylinositols (PI), phosphatidylserines (PS), phosphatidylethanolamines (PE), and phosphatidylglycerols (PG) along with several other glycosphingolipids and cardiolipins (CL) are observed in negative ion mode.[22] Dual polarity lipid analysis of the same tissue section could help to resolve this issue.[19] For this purpose, matrix compounds that provide efficient ionization in both polarities, such as 1,5-DAN,[18] DHB,[21] and DHAP[23] are required. The particular advantage of 1,5-DAN as a matrix is its low ionization energy[18] and sensitivity for lipid molecules, which provides high spectral quality at low laser fluence[20] and in turn results in minimized laser ablation-induced tissue distortions as visualized by subsequent immunofluorescence staining.[20] This "gentle" desorption/ionization process, particularly in negative mode, allows for preservation of tissue morphology and shows minimal mechanical tissue distortion, respectively, along with limited consumption of lipids. This facilitates efficient subsequent lipid analysis in positive ion mode on the very same raster spot.

In order to investigate the performance of subsequent, multimodal lipid MALDI imaging mass spectrometry on the same imaging pixel array, cerebellar regions in sagittal mouse brain tissue were analyzed (Figure 1, Supporting Information Figure S-1). Here, the impact of laser fluence was studied using different numbers of laser shots (5, 10, 20, 30, 50, 100) in negative ion mode, followed by IMS in positive polarity on the same pixel points using a constant number of laser shots (n = 50). The number of laser shots in positive ion mode was optimized before on a nonpre-analyzed, cerebellar area, equivalent in size and morphology (Supporting Information Figure S-1d–f).[20]

When applying this approach for negative ion mode analysis, the total signal intensity of lipids over a mass range of 300–2000 Da, while excluding all matrix peaks, displayed a significant decrease as soon as the number of laser shots was increased beyond 10 (Figure 1a). This was accompanied by a significant increase in total ion intensity of matrix-derived signals, most prominent between 300 and 650 Da. (Figure 1b, Supporting Information Figure S-1a–c), indicating a reduced lipid ionization efficiency (Figure 1a,b). This is further illustrated when considering the ratio of total negative ion lipid intensity (300–2000 Da, excluding matrix peaks) and total matrix peak intensity (300–650 Da), where the steepest slope is observed between a stepwise increase from 10 to 20 laser shots (Figure 1c).

The low-ionization energy of 1,5-DAN[18] allows enhanced ionization of lipid species at small laser focus parameters without the need of high laser pulse energies and number of laser shots (Supporting Information Figure S-1).[20] On the other hand, for analysis in both polarities, an increasing number of laser shots results in lipid ion suppression due to formation of excessive amounts of matrix- ions and -clusters in the ablation plume (Supporting Information Figure S-1a–f). This is explained by the fact that sublimation results in smaller crystals that in turn result in higher temperatures during the nanosecond laser desorption/ionization process as the smaller crystal lattices do not allow for heat dissipation.[24] This effect results in both enhanced analyte- and matrix ionization. 1,5 DAN forms radicals upon laser irradiation that in turn result in matrix cluster formation. Therefore, when higher laser fluences are applied and thereby higher temperatures are generated in the ablation plume, extensive cluster formation is observed, which in turn results in analyte suppression.[24]

It is therefore crucial to optimize the laser fluence, to minimize matrix suppression effects in order to facilitate efficient lipid ionization. Moreover, minimizing cluster formation provides improved spectral coverage ($<m/z$ 650) and detection of physiologically relevant lipid signals, including, e.g., ceramides (Cer), due to less convolution by matrix cluster ion peaks in the corresponding mass region (Supporting Information Figure S-1g–j).[20]

In addition to these effects, increased laser power can result in spatial overlapping effects that compromise sensitivity and spatial resolution.

In general, when using 1,5-DAN, spectral data were found to be more complex and intense in negative ion mode as compared to positive ion mode data, including more prominent matrix clusters signals (Supporting Information Figure S-1a–f).[5,20] This can be attributed to distinct reductive properties and radical ion transfer abilities of 1,5-DAN[18] as compared to several other matrixes.[5,20] Indeed, 1,5-DAN as a basic matrix compound can act as a "proton sponge" in the gas phase which can partially suppress protonation of lipids. In addition, as only a few number of low-energy laser shots are required for desorption and ionization in negative ion mode, plasma shielding effects are minimized.[25−27] These plasma shielding effects occur, when a high numbers of laser shots are used at high repetition rates and lead to absorption, scattering, and diffuse reflection of incident laser light by the ablation plume, which in turn can result in reduced ablation efficiency and lipid ionization sensitivity.

Using low number of shots in negative ion mode, as facilitated by the superior ionization sensitivity of 1,5-DAN, results further in minimized-mechanical distortion and consumption of lipids on a given coordinate of matrix-coated tissue.[20] Beyond the reduced spectral convolution, allowing detection of physiologically relevant lipids below 650 Da, the use of low numbers of laser shots also allows for sensitive, subsequent analysis in positive ion mode on the same imaging region and even on the same pixel points.

Indeed, the total ion intensity of positive lipid signals (300–2000 Da, excluding matrix signals) acquired from the exact same imaging MS pixel array showed maintained high intensity after 5–10 laser shots in the preceding negative ion mode analysis, as compared to a nonpre- irradiated tissue area (Figure 1d). In contrast, a characteristic decrease of total positive lipid intensity, as well as matrix signal, was observed after the acquisition of 10 laser shots in preceding negative ion mode analysis (Figure 1d,f), indicating overall decreased spectral quality. This can be explained by the increased mechanical ablation and consumption of lipid and matrix molecules along with the distortion of matrix-coating, which could impair laser desorption/ionization geometry for subsequent laser shots on

DOI: 10.1021/acschemneuro.7b00314
ACS Chem. Neurosci. 2017, 8, 2778–2790

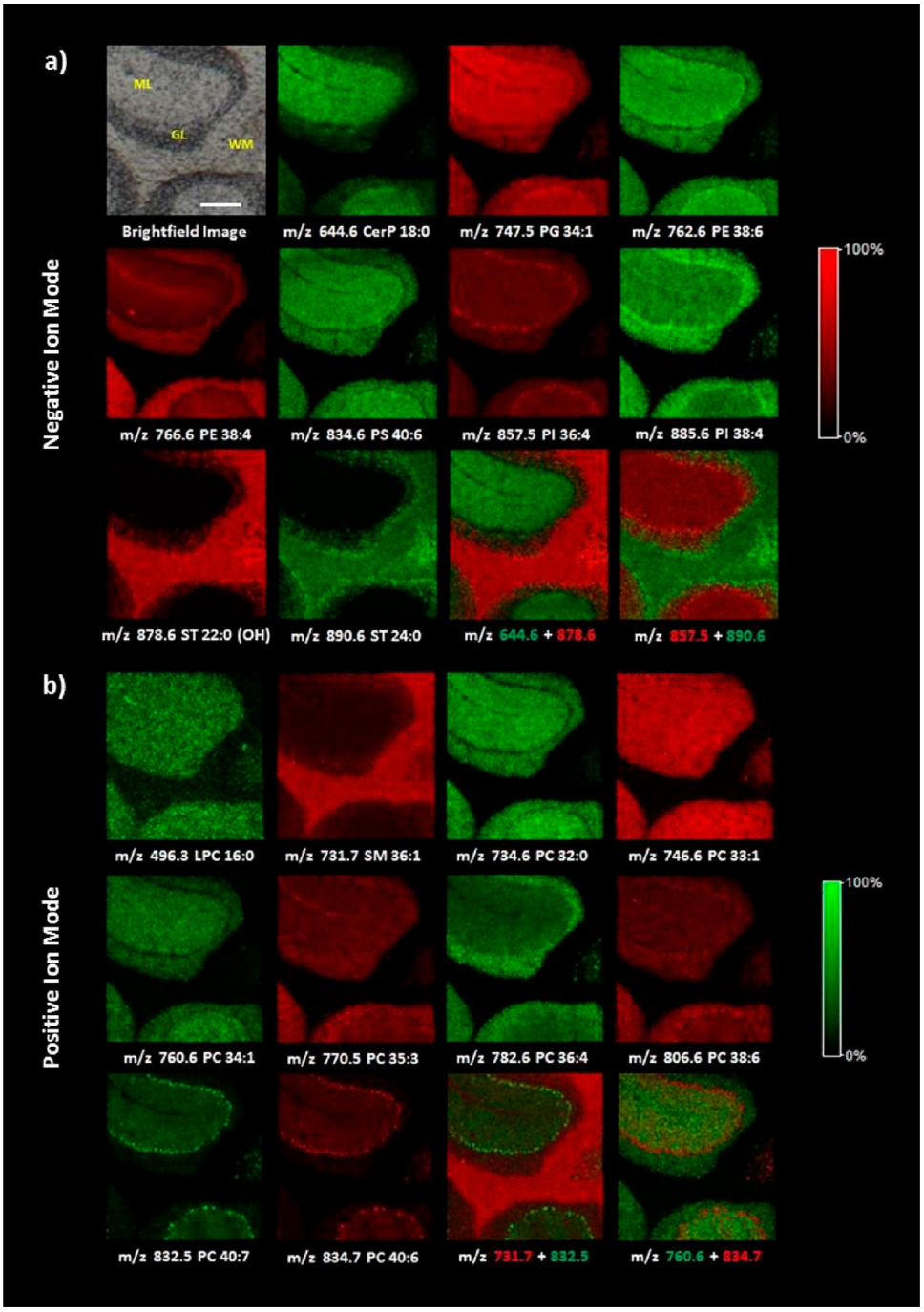

Figure 2. High-resolution, dual polarity MALDI-IMS of lipids on the same pixel points in the cerebellum in sagittal mouse brain sections. IMS data were collected both in (a) negative and (b) positive ion mode with a lateral resolution of 10 μm at the same pixel points. (a) In negative ion mode, ceramide 1-phosphates (CerP 18:0), phosphatidylglycerols (PG 34:1), phosphatidylethanolamines (PE 38:4, PE 38:6), phosphatidylserines (PS), and phosphatidylinositols (PI) were found to localize to the molecular layer (ML) and granular layer, while sulfatides (ST 22:0 (OH), ST 24:0) localized to white matter (WM). (b) In positive ion mode, lysophospatidylcholines (LPC 16:0) and phosphatidylcholines (PC 32:0, PC 33:1, PC 34:1, PC 35:3, PC 36:4, PC 38:6) were detected in both GL and ML or selectively in the ML (as for PC 40.6, PC 40:7). In contrast, sphingomyelin (SM 36:1) was selectively observed in WM. Scale bar: 200 μm.

the given coordinates and result in generally decreased spectral quality.

Finally, considering the structured beam profile of the smart beam laser[28] used in these experiments, an increasing number of laser pulses can also result in inhomogeneous ablation profiles on the matrix-coated brain tissue. The following laser desorption on the same pixel points can result in an inhomogeneity of the subsequent laser-desorption plumes, which is reflected in an increased standard deviation of the total signal intensities of lipids and matrix in positive ion mode on the same raster spots as observed in the present study (Figure 1a,d and b,e).

Taken together, the optimization steps of dual polarity lipid imaging MS revealed that a number of 10 laser shots in the first IMS stage perfomed in negative mode provides high spectral quality in both subsequent IMS stages, while higher laser

DOI: 10.1021/acschemneuro.7b00314
ACS Chem. Neurosci. 2017, 8, 2778−2790

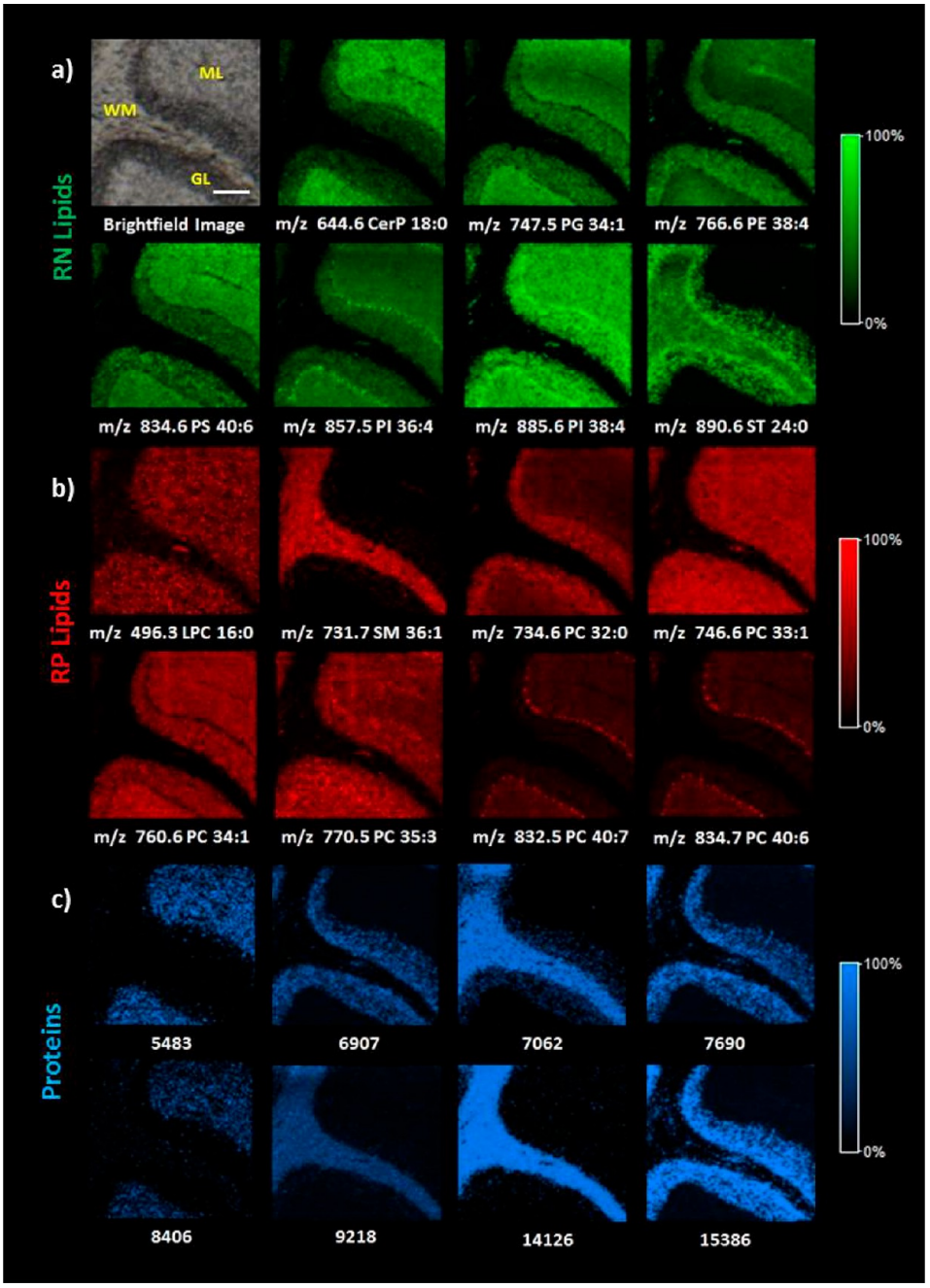

Figure 3. High-resolution (10 μm), trimodal MALDI imaging MS data acquired on the same IMS region in mouse cerebellum. (a,b) Dual polarity MALDI-IMS of lipids in negative ion mode a) and b) positive ion mode was followed by high-resolution (10 μm) protein imaging on the same IMS region (c). Protein signals were attributed based on accurate mass and literature values,[31] including: m/z 5483 cytochrome *c* oxidase 7c (Cox7c); m/z 6907 histone H2B $[M+2H]^{2+}$; m/z 7062 myelin basic protein (MBP) 14 kDa $[M+2H]^{2+}$; m/z 7690 histone H3 $[M+2H]^{2+}$; m/z 9218 MBP 18 kDa $[M+2H]^{2+}$; m/z 14 126 MBP 14 kDa; m/z 15 386 histone H3. m/z 8406 could not be attributed; WM, ML, and GL represent white matter and molecular and granular layers, respectively (a). Scale bar: 200 μm.

fluences lead to decreased lipid signals and higher matrix intensity for the negative ion mode analysis. Moreover, the matrix preparation is affected for subsequent positive ion mode IMS, resulting in generally decreased spectral quality. Similarly, higher numbers of laser shots (>50) in the second stage, positive ion mode IMS, result in decreased lipid signal and increased matrix cluster formation (Supporting Figure S-1e,f).

Following the optimization experiments, we performed high-resolution (10 μm) dual polarity lipid imaging of cerebellar regions on sagittal mouse brain sections (Figure 2). Here, lipid ion images in both negative and positive polarities could be simultaneously visualized for the specific cerebellar regions, including cerebellar -white matter, granular- and molecular-layers (Figure 2a,b).

For example, inspection of lipid ion imaging data acquired in negative mode at 10 μm resolution showed that ceramide 1-phosphates (CerP 18:0) localized densely to the cerebellar molecular layer, whereas phosphatidylinositols (PI 38:4 and PI 36:4), as well as phosphatidylethanolamines (PE 38:4), were detected in both the granular and molecular layers where PI 38:4 was particularly elevated in the Purkinje cell layer. In contrast, sulfatides (ST 22:0(OH), ST 24:0) localized to the

DOI: 10.1021/acschemneuro.7b00314
ACS Chem. Neurosci. 2017, 8, 2778−2790

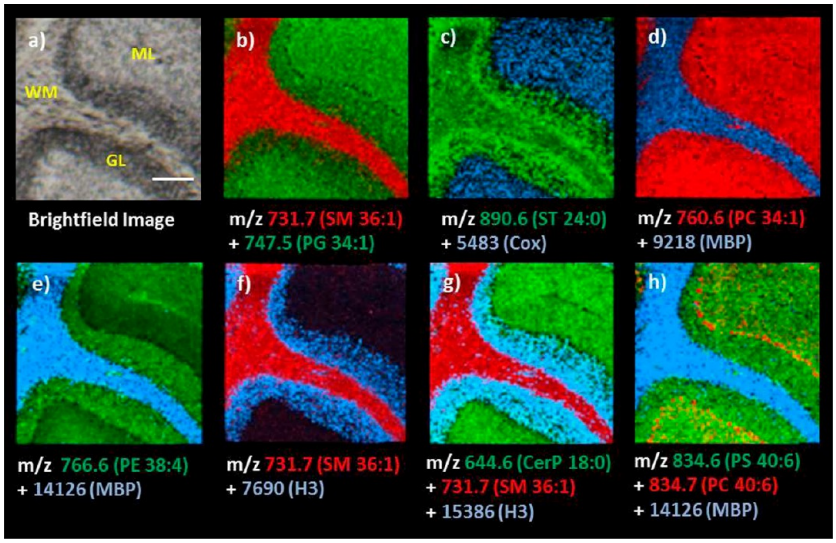

Figure 4. Overlaid multimodal ion images for lipids acquired in negative (green) and positive (red) ion mode together with proteins signals (blue) obtained on the same region in the cerebellum. The data display the same cerebellar area of a sagittal mouse brain section as illustrated in Figure 3. (a) Bright field image, outlining the major cerebellar areas including the white matter (WM), granular (GL) and molecular layer (ML). (b) Overlay images of dual polarity lipid signals for SM 36:1 (red, m/z 731.7) and PG 34:1 (green, m/z 747.5). (c–h) Overlay images for multimodal imaging data including lipid- and protein-signals: (c) ST 24:0 (green, m/z 890.6) and Cox7c (blue, m/z 5483); (d) PC 34:1 (red, m/z 760.6) and MBP (blue, m/z 9218, $[M+2H]^{2+}$); (e) PE 38:4 (green, m/z 766.6) and MBP (blue, m/z 14126); (f) SM 36:1 (red, m/z 731.7) and histone H3 (blue, m/z 7690 $[M+2H]^{2+}$); (g) CerP 18:0 (green m/z 644.6), SM 36:1 (red, m/z 731.7), and histone H3 (blue, m/z 15386; (h) MBP (blue, m/z 14126), PS 40:6 (green, m/z 834.6), and PC 40:6 (red, m/z 834.7). Scale bar: 200 μm.

white cerebellar matter region. (Figure 2a) Lipids acquired in positive ion polarity, such as lysophosphatidylcholines (LPC 16:0) and phosphatidylcholines (PC 32:0, PC 33:1, PC 34:1, PC 35:3, PC 36:4, PC 38:6) were detected in both granular and molecular layers, whereas SM 36:1 was selectively observed in the white matter (Figure 2b). Moreover, PC 40:7 and PC 40:6 species were lower in the granular layer but characteristically abundant in the Purkinje cell layer, while PC 32:0 and PC 34:1 were selectively depleted in that region (Figure 2b).

Dual Polarity Lipid MALDI-IMS Followed by Protein MALDI-IMS on the Same Imaging Region at 10 μm Spatial Resolution. The diversity of molecular target species and the mass range of different MALDI IMS analyses modes are directly related to the choice of matrix compounds and their compatibility with matrix application strategies. Therefore, subsequent multimodal MALDI IMS analysis of lipids and proteins typically requires the use of multiple matrix compounds and corresponding tissue washing and matrix deposition procedures.

We here investigated the potential of a trimodal, repeat MALDI IMS approach at 10 μm spatial resolution to probe the distribution of lipids and proteins on the same imaging area within the same tissue section. For that, we used the previously described histology-compatible MALDI-IMS[20] approach based on 1,5-DAN matrix sublimation[5] for dual polarity MALDI-IMS of lipids (Figure 2). This was followed by MALDI IMS of proteins on the same region within the mouse cerebellum previously analyzed for lipids (Figure 3). MALDI imaging of proteins was based on 2,5-dihydroxyacetophenone (2,5-DHA), which was previously demonstrated to be a highly sensitive and adequately vacuum stable matrix compound for MALDI IMS of proteins.[29,30] This workflow, however, results in tissue surface distortion, due to higher laser fluence needed for protein ionization and consequently laser-induced, mechanical stress as revealed by subsequent H&E staining, which does not allow for subsequent histological immunostaining experiments. (Supporting Information Figure S-2). Despite this limitation, the here demonstrated trimodal imaging paradigm allows identification of colocalizing lipid (Figure 3a,b) and protein signals (Figure 3c), acquired from the same imaging region.

As illustrated by an overlay of individual ion intensity patterns from the trimodal imaging data, this method allowed to elucidate corresponding and complementary chemical distribution patterns with respect to anatomical regions of interest, including the cerebellar white matter, granular layer and molecular layer (Figure 4a–h).

For example, sphingomyelins (SM 36:1, m/z 731.7) detected in positive ion mode and expressed in the white matter could be overlaid with phosphatidylglycerols (PG 34:1, m/z 747.5) detected in negative ion mode and expressed in granular and molecular layers, demonstrating the complementary distribution of multimodal imaging data (Figure 4b). Protein signals for, e.g., cytochrome c oxidase 7c (Cox7c, m/z 5483, Figures 3c and 4c), and myelin-basic protein (MBP, m/z 9218, $[M+2H]^{2+}$, Figures 3c and 4d) that localized to the molecular layer and white matter, respectively, were overlaid with lipids, including sulfatides (ST 24:0, m/z 890.6, white matter, Figure 4c) acquired in negative ion mode and phosphatidylcholines (PC 33:1, m/z 746.6, molecular layer, Figure 4d) acquired in positive ion mode that displayed similar or complementary localization pattern. Similarly, MBP 14 kDa and PE 34:1 localized complementarily to white matter and molecular layer, respectively (Figure 4e).

An overlay of SM 36:1 (m/z 731.7) and histone H3 (m/z 7690, $[M+2H]^{2+}$) highlights the distinct localization of histone H3 to the granular layer (Figure 4f). This can be attributed to the cell nuclei in the cell body rich granular layer as these contain larger amounts of histones that stabilize chromatin in the cell nuclei. Triple overlay data further demonstrate how ceramides (CerP 18:0, m/z 644.6) and sphingomyelins (SM

DOI: 10.1021/acschemneuro.7b00314
ACS Chem. Neurosci. 2017, 8, 2778–2790

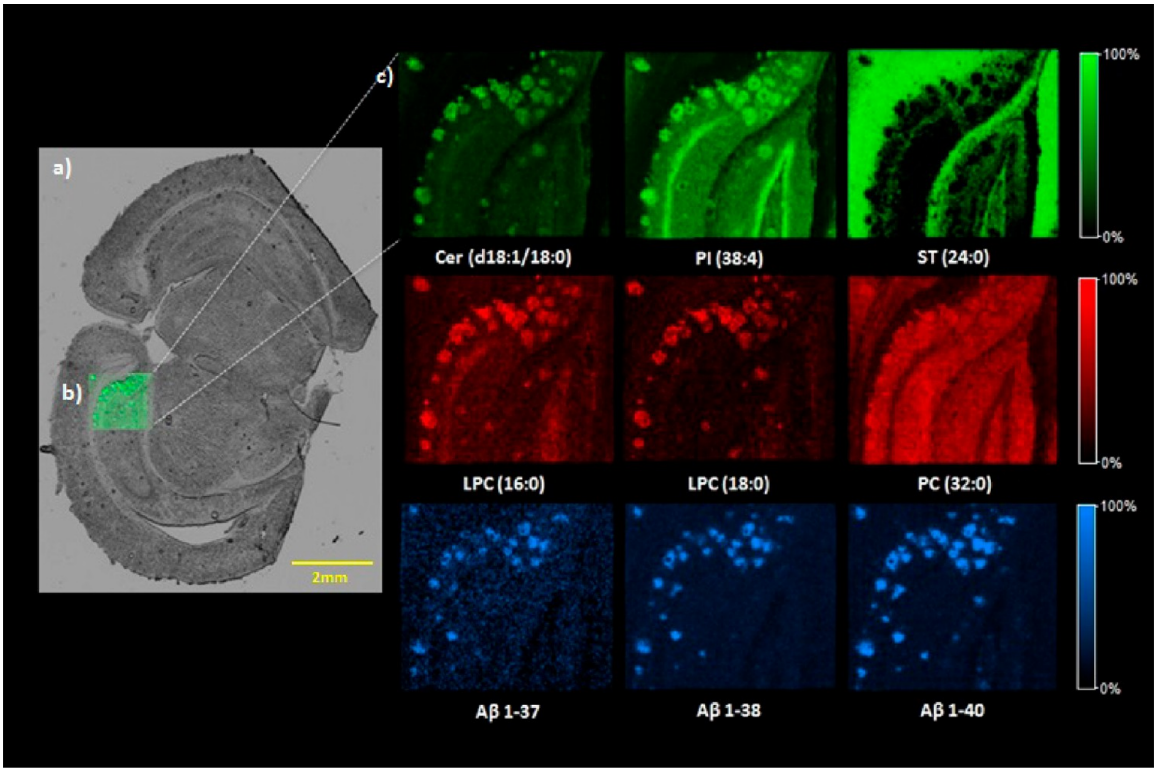

Figure 5. Hippocampal amyloid plaque-associated lipids in dual polarity and peptides (a) on a coronal mouse brain tissue section of transgenic AD mice (tgArcSwe) were revealed by multimodal MALDI-IMS. (b) Hippocampal region analyzed with 10 μm spatial resolution. (c) Ion images of lipids: ceramides (Cer d18:1/18:0, m/z 564.6), phosphatidylinositols (PI 38:4, m/z 885.6), sulfatides (ST 24:0, m/z 890.6) acquired in negative (green) and lysophosphatidylcholines (LPC 16:0, m/z 496.3, LPC 18:0, m/z 524.3) and posphatidylcholines (PC 32:0, m/z 734.6) acquired in positive (red) ion mode with subsequently acquired amyloid-β (Aβ 1−37, m/z 4002.7, Aβ 1−38, m/z 4060.3, Aβ 1−40, m/z 4257.6) peptide (blue) ion images within the same imaging region.

36:1, m/z 731.7) are expressed in the molecular layer and white matter, respectively, while histone H3 (m/z 15386, $[M+H]^+$) localizes characteristically to the granular layer (Figure 4g). Similarly, an overlay of MBP, PS 40:6 and PC 40:6 highlights a complementary localization to the white matter (MBP), molecular layer (PS) and the Purkinje cell layer (PC) (Figure 4h). Here, the high spatial resolution of this methodology allows visualizing individual neuronal cell bodies in the Purkinje cell layer as outlined by localization of PI 36:4 (Figure 3a) and PC 40:6 and 40:7 (Figures 3b and 4h). These results highlight the potential of trimodal MALDI imaging to probe biochemical correlates of pathohistological features at cellular scales. Consequently, this method provides a powerful approach to correlate lipid and protein localizations to histopathological features including abnormal protein aggregation characteristic for neurodegenerative diseases like, e.g., Alzheimer's (AD), Parkinson's (PD), or prion diseases in order to probe the complex chemical interactions underlying proteopathy in these diseases.[32]

High-Resolution (10 μm) Multimodal MALDI-IMS Reveals Amyloid Plaque-Associated Lipids and Aβ Isoforms in Transgenic Alzheimer's Disease Mice (tgArcSwe). The neuropathology of AD is characterized by loss of memory and cognition as a consequence of progressive neuronal degeneration. This has been suggested to be due to impairment of hippocampal synaptic efficacy caused in part by diffusible extracellular amyloid-β (Aβ) aggregates.[33,34] Aβ accumulation has been suggested to trigger AD pathogenesis,[34] where Aβ peptides rapidly aggregate to form oligomers, protofibrils, and fibrils, eventually leading to the formation of extracellular plaques.[35] However, the molecular mechanisms of this process are not fully understood. A number of studies suggest that, along with Aβ peptide-related mechanisms, several lipid species including cholesterol,[36,37] sphingolipids,[20,38−40] and phospholipids[40−42] can have prominent roles in Aβ plaque pathology in AD.[39,43] Therefore, high-resolution multimodal, chemical imaging methods can be a powerful strategy to disentangle the multiple aspects of molecular amyloid pathology in situ.

Our group has previously studied the expression pattern of amyloid plaque-associated Aβ peptides[44] and sphingolipids[20,38] in transgenic AD mice (tgArcSwe and tgSwe) using multimodal chemical imaging strategies. Therefore, we employed the here described comprehensive multimodal MALDI-IMS approach to delineate the distribution patterns of positively and negatively charged lipid species along with the Aβ peptide isoforms associated with amyloid plaque pathology in transgenic AD mice (tgArcSwe) (Figure 5). This mouse model carries both the Arctic (E693G) and the Swedish (K670M/N671L) mutation and displays extensive Aβ deposition with an early onset age of 5−6 months. It is, therefore, a well-suited model system to study Aβ pathology.[45] We performed trimodal MALDI-IMS on 18-month-old tgArcSwe mice brain tissue sections for comprehensive lipid and peptide imaging to elucidate Aβ plaque associated localizations/alterations of lipid species potentially implicated in AD pathology. Indeed, the results reveal a prominent colocalization for various lipid

DOI: 10.1021/acschemneuro.7b00314
ACS Chem. Neurosci. 2017, 8, 2778−2790

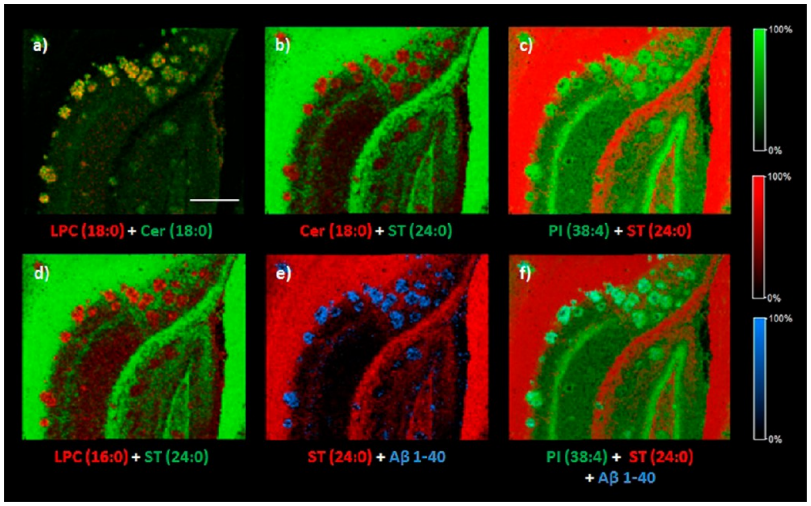

Figure 6. Overlaid images of hippocampal amyloid plaque-associated lipids and amyloid peptides in Figure 5. (a) LPC (18:0) and Cer (18:0), (b) Cer (18:0) and ST (24:0), (c) PI (38:4) and ST (24:0), (d) LPC (16:0) and ST (24:0), (e) ST (24:0) and Aβ 1−40, and (f) PI (38:4), ST (24:0) and Aβ 1−40. Scale bar: 250 μm.

species analyzed in dual polarity and several amyloid-β peptides (Figure 5).

Inspection of the ion images revealed that lipids obtained in negative polarity (green), including ceramides (Cer d18:1/18:0, m/z 564.6), phosphatidylinositols (PI 38:4, m/z 885.6) and sulfatides (ST 24:0, m/z 890.6), display strong colocalization with ion images of lipids obtained in positive polarity (red), including lysophosphatidylcholines (LPC 16:0, m/z 496.3, LPC 18:0, m/z 524.3) and posphatidylcholines (PC 32:0, m/z 734.6) (Figure 5c). Moreover, a strong colocalization of the lipid accumulations was observed with intensity distributions of various amyloid β peptides (blue) (Aβ 1−37, m/z 4002.7, Aβ 1−38, m/z 4060.3, Aβ 1−40, m/z 4257.6) (Figure 5c).

An overlay of the trimodal IMS data revealed that plaque feature-like localization patterns observed for various lipid species were shown to be attributed to the Aβ plaques as verified by the peptide imaging data (Figure 6). Furthermore, immunohistochemistry (IHC) staining was performed using a monoclonal Aβ antibody (Aβ1−16, 6E10) following MALDI-IMS analysis of lipids in negative ion mode, which further verified the amyloid identity of the aggregates (Supporting Information Figure S-3). As a further control, MALDI-IMS data for negative ion mode lipids were collected in the hippocampal region of 18-month-old control, wild-type mice to verify that the lipid accumulations observed are related to amyloid plaque pathology. Here, no plaque-like accumulation patterns or general elevations were observed for the lipid species that show plaque localization in transgenic mice (Supporting Information S-4). This further verifies the relevance of the here observed lipid distribution in Aβ pathology.

Aβ plaque-associated ceramide elevation and sulfatide deficiency, as observed here, was previously described for the same transgenic mouse model (tgArcSwe) using MALDI-IMS.[38] Here, the same phenomenon was observed explicitly at high-spatial resolutions. (Figure 6b) Moreover, shotgun lipidomics studies of transgenic AD mice and human AD brain homogenates consistently indicated the same results.[46] Sulfatides are highly enriched in myelin sheaths and mainly synthesized by oligodendrocytes playing key roles in the regulation of oligodendrocyte maturation and myelin formation.[47] Indeed, it has been hypothesized that alterations of apolipoprotein E (APOE) ε4 allele-mediated sphingolipid homeostasis through lipoprotein metabolism pathways can lead to depletion of sulfatides in AD pathogenesis.[48] Moreover, the substantial increase in ceramide content are suggested to be a potential result of sulfatide degradation, but other explanations include membrane-associated oxidative stress[37] or accelerated hydrolysis of sphingomyelin.[46,49] Indeed, oligondendrocytes are highly susceptible to oxidative stress possibly due to the demanding energy for the production of lipid-rich and protein-dense myelin sheaths.[50,51] Therefore, amyloid plaque-associated perturbation of sulfatide homeostasis can be associated with the regression of myelination, which is another pathological hallmark of Alzheimer's disease.[52]

The increase in lysophosphatidylcholines (LPC) and decrease in phosphatidylcholines (PC) have been previously reported in hippocampus, cortex and subiculum of another transgenic AD mice (5XFAD) using MALDI-IMS.[41] Further, immunostaining of PLA_2 showed partial PLA_2 localization around amyloid plaques.[41] This suggests an amyloid-plaque associated hyperactivity of PLA_2, which causes amyloid-associated alterations of LPCs and PCs. Indeed, Aβ exerts its cytotoxic effects mainly perturbing cellular membranes, partially through the modulation of the activity of phospholipases, such as PLA_2[53] and PLC.[54] Moreover, increased neuronal activity of PLA_2 converts PC to LPC, which stimulates glial cells and subsequently induces neuroinflammation.[55] Our high-spatial-resolution, trimodal MALDI-IMS approach reveals amyloid plaque-associated elevations of LPCs which is directly correlated with sphingolipids on the same plaques (Figure 6a,d). On the other hand, the plaque specific elevation of lysophosphatidycholines can be attributed to their roles in Aβ oligomerization and fibril formation.[42,56] Finally, it is also well-known that LPC induces demyelination via glial LPA signaling.[57] This further links LPC localization to plaque-associated demyelination as observed in AD,[52] which is in line with the plaque-associated sulfatide dyshomeostasis.[38]

We further observed a significant elevation of phosphatidylinositols (PI 38:4, m/z 885.6) on amyloid plaques (Figure 6c,f). Interestingly, while previous reports described a general reduction of these species in hippocampus and cortex tissue of human AD brains,[58,59] we observed a plaque specific increase.

DOI: 10.1021/acschemneuro.7b00314
ACS Chem. Neurosci. 2017, 8, 2778−2790

While this can be due to possible differences in amyloid pathogenesis of human AD and transgenic AD mice (tgArcSwe), our approach reports spatially resolved localizations of these species to Aβ plaques at 10 μm spatial resolution (Figure 6c,f). Previous findings are based on brain extracts and therefore lack the spatial aspect of analysis, making pathology specific correlation analysis impossible. Indeed, PI lipids were previously identified to play a role in amyloid fibril growth.[60] Moreover, an AD-associated reduced phosphatidylinositol kinase activity[61] along with the dysregulated phosphatidylinositol-4,5-bisphosphate metabolism by oligomeric amyloid-β peptide[54] were previously reported, which could be possible pathways for plaque-associated PI elevation. This highlights the potential of the here employed high-resolution, multimodal MALDI-IMS approach that allows for simultaneous analysis of lipids and peptides in a single microscale Aβ plaque region within a specific brain area (Figures 5 and 6).

On the other hand, this approach suggests an improved strategy for validation of the amyloid identity of Aβ aggregates, as compared to immunohistochemical assessment. This is due to the limitations of antibody-based approaches with respect to specificity and comprehensiveness, as IHC only allows for simultaneous detection of one or two relevant Aβ isoforms at sometimes questionable specificity.[38,44] In contrast, the here presented approach offers a possibility to correlate multiple isoforms at once with high chemical specificity. This is further inferred, with the possibility for in situ validation through MS/MS experiments.

In Situ MS/MS Based Identification of Aβ Plaque-Associated Lipids and Peptides. In MALDI, fragmentation strategies such as collision induced dissociation (CID),[62] post source decay (PSD),[63] and in-source decay (ISD)[64] have been used for in situ identification of analytes directly on the tissue section. However, in situ MALDI MS/MS using PSD, as enabled on a TOF/TOF instrument, is challenging due to suppression effects and the lower fragmentation efficiency of PSD. This approach is therefore, time-consuming and requires a lot of laser shots for spectra acquisition, resulting in increased consumption of analyte and matrix, which in turn facilitates only a few MS/MS experiments. However, histopathological accumulations of certain lipid- and amyloid peptide species on plaques or other histological features provide a natural preconcentration, enabling efficient MS/MS analysis on plaque aggregates in situ. The potential of this approach for in situ identification of neuronal lipid species was previously demonstrated by our group.[20,38] Therefore, we applied MALDI MS/MS analysis in LIFT-TOF/TOF mode for lipids and peptide fragmentation following MALDI-IMS analysis of the corresponding modality (Figure 7).

The results demonstrate the potential of this approach for in situ identification of lipids and peptide including Cer (d18:1/18:0) and Aβ 1−40, directly on plaque aggregates. Here, diagnostic fragment ions for Cer (d18:1/18:0) (Figure 7a) and other plaque-associated neuronal lipids (Supporting Information Figure S-5) allowed identification of the corresponding lipid species. Moreover, for MS/MS analysis of Aβ 1−40 a multitude of sequence specific b- and y-fragment ions were detected (Figure 7b), yielding a high-degree of confidence in the sequence identity (Supporting Information Figure S-6). The here presented multimodal MS/MS data further highlight the potential of the approach for comprehensive, molecular analysis of complex biological tissues with high chemical specificity.

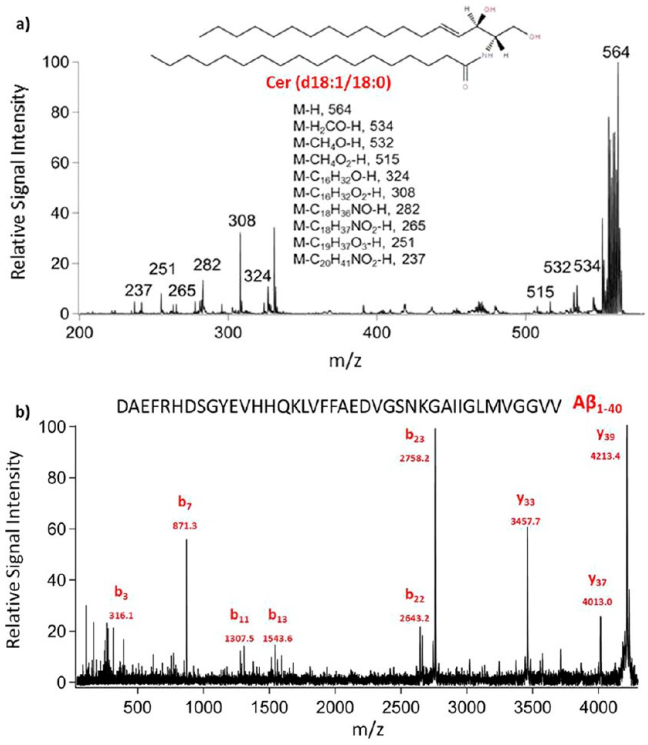

Figure 7. Multimodal tandem mass spectrometry of lipid and peptide species in situ. MS/MS acquisition on plaque features as exemplified for (a) Cer (d18:1/18:0, m/z 564.6) and (b) Aβ (1−40, m/z 4257.6). Diagnostic fragment ions are annotated for Cer (d18:1/18:0) (a) as well as sequence specific N-terminal (b) and C-terminal (y) fragment ions for Aβ 1−40, allowing unambiguous identification of lipids and peptides in situ.

CONCLUSIONS

We here present a trimodal MALDI-IMS paradigm that allowed for subsequent acquisition of lipid data in positive and negative polarity from the same pixel point followed by protein imaging all at 10 μm spatial resolution. This enabled identification of colocalizing lipids and protein species within the same tissue section. The results demonstrate the potential of this approach for comprehensive molecular imaging of cerebellar lipid and protein species, delineating histological features and anatomical regions of interest. Moreover, an application to a transgenic mouse model of AD (tgArcSwe) revealed amyloid plaque-associated lipid species that were colocalized with distinct Aβ peptide isoforms. Therefore, this approach can substantially increase the potential for multimodal MALDI imaging MS to comprehensively probe neurodegenerative disease pathologies in situ.

METHODS

Chemicals and Reagents. All chemicals for matrix and solvent preparation were pro-analysis grade and obtained from Sigma-Aldrich (St. Louis, MO), unless otherwise specified. TissueTek optimal cutting temperature (OCT) compound was purchased from Sakura Finetek (AJ Alphen aan den Rijn, The Netherlands). The ddH2O was obtained from a Milli-Q purification system (Merck Millipore, Darmstadt, Germany).

Animals. C57BL/6 female mice from Charles Rivers Laboratories were used for method development (Sulzfeld, Germany). The animals were housed at the animal facility in Gothenburg (Laboratory of Experimental Biomedicine, EBM), kept under standard conditions of daylight (12 h light cycle), and provided with food and water ad

DOI: 10.1021/acschemneuro.7b00314
ACS Chem. Neurosci. 2017, 8, 2778−2790

libitum. Animals were delivered with their respective dams that were further separated at postnatal day (PND) 21 of the pups. Transgenic mice, 18 months of age, with the Arctic (E693G) and Swedish (K670N, M671L) mutations (tgArcSwe) of human APP were reared ad libitum at the animal facility at Uppsala University under a 12 h/12 h light cycle. All animal procedures were approved by an ethical committee and performed in compliance with national and local animal care and use guidelines (DNr #C17/14 at Uppsala University).

Tissue Collection and Sectioning. The animals were anesthetized with isoflurane and sacrificed by decapitation. The brains were dissected quickly with 3 min postmortem delay and frozen on dry ice. Frozen tissue sections (12 μm thick) were cut in a cryostat microtome (Leica CM 1520, Leica Biosystems, Nussloch, Germany) at −18 °C, and collected on indium tin-oxide (ITO) coated conductive glass slides (Bruker Daltonics, Bremen, Germany) and stored at −80 °C.

MALDI IMS Sample Preparation and Matrix Application. Prior to matrix application, tissue sections were thawed in a desiccator for ∼30 min under reduced pressure (SpeedVac, Eppendorf, Hamburg, Germany). The ITO glasses were marked with a glass cutter (Starwalker, Montblanc, Germany) to give sharp-edged cross features for the teaching of the navigation points in the MALDI imaging acquisition software (Flex Imaging, v3.0, Bruker Daltonics). The mounted tissue sections were scanned in a histology slide scanner (PathScan Enabler IV, Electron Microscopy Sciences, Hatfield, PA). Matrix deposition for lipid analysis was carried out by sublimation of 1,5-diaminonaphthalene (1,5-DAN) using a vacuum sublimation apparatus (Sigma-Aldrich). The sublimation chamber was connected to a membrane vacuum pump (Jula, Skara, Sweden) attached to a digital vacuum gauge controller and placed in a heated sand bath (SiO_2, 50−70 mesh particle size, Sigma-Aldrich) on a hot plate (C-MAG HP 4, IKA Werke GmbH & Co. KG, Staufen, Germany) and connected to an electronic contact thermometer (ETS-D5, IKA Werke GmbH & Co. KG, Staufen, Germany). Sublimation was performed by the following steps. First, thawed and vacuum-dried (∼20 min) ITO-glass slides with the thaw-mounted mouse brain tissues were attached to the flat top of the chamber using double-sided heat conductive copper tape. Then, ∼300 mg of 1,5 DAN matrix powder was placed evenly on the outer bottom of the sublimation chamber, which was then attached to the top using the O-ring seal. A reduced pressure of 0.8 mbar was applied and the system was allowed to equilibrate under vacuum for a period of ∼20 min. The sand bath temperature was set to 130 °C. The cooler was filled with ice slush (≥0 °C) for condensation of the matrix on the sample slides. The sublimation time was 20 min. The process was halted by removing the sublimation apparatus from the sand bath and closing the vacuum valve. The sublimation apparatus was allowed to slowly re-equilibrate to atmospheric pressure before removal of the sample plate. The amount of deposited matrix on ITO glass was determined using a high-precision scale (AX224, Sartorius, Göttingen, Germany) weighing the amount before and after the sublimation experiments. The sublimation protocol was optimized with respect to temperature, deposition time and the total amount of deposited matrix to obtain the best detection efficiency for lipids on mouse brain tissue. With this setup, the optimum matrix layer was found to be 120 $\mu g/cm^2$ to give the best lipid signals.[20] Here, a too thin matrix layer (50−70 μg/cm2) yielded very few lipid ions, while a too thick matrix layer (200−300 μg/cm2) resulted in dominant matrix ions (Supporting Information S-7).

Prior to protein imaging, tissue sections were washed 2× 100% ethanol (EtOH) (30s) to remove the remaining 1,5-DAN matrix. Lipids and salts were washed away in sequential washes of 70% EtOH (30 s), 100% EtOH (30 s), Carnoy's fluid (6:3:1 EtOH/chloroform:-acetic acid) (2 min), 100% EtOH (30 s), H_2O with 0.2% TFA (30 s), and 100% EtOH (30 s).[65]

The teaching of the navigation points was performed using the same sharped-edged cross points created with the glass cutter pen in the preceding lipid analysis to minimize the repositioning error between lipid and protein imaging mass spectrometry analysis. 2,5-Dihydroxyacetophenone (2,5-DHA) was used as matrix compound and applied using a TM Sprayer (HTX Technologies, Carrboro, NC, USA) combined with a HPLC pump (Dionex P-580, Sunnyvale, CA, USA). Before every spraying experiment, the solvent pump valve was purged first manually using a syringe followed by the implemented automatic purging function for ∼10 min. The pump was then kept running at isocratic flow with 100 μL/min using 70% ACN as pushing solvent for 3 h. A matrix solution of 15 mg/mL 2,5-DHA in 60% ACN/1% CH_3COOH/1%TFA was sprayed onto the tissue sections using the following instrumental parameters: nitrogen flow (10 psi), spray temperature (75 °C), nozzle height (40 mm), eight passes with offsets and rotations, and spray velocity (1300 mm/min). Following the matrix deposition, the preparations were recrystallized as described previously.[65] Here, the slides were mounted with copper tape on a top of a Petri dish (100 mm diameter × 15 mm deep, VWR, Stockholm, Sweden) with a filter paper pipetted with 5% methanol and placed on the lower part of the dish. The glasses were closed and placed in an oven at 85 °C for 3.5 min.

MALDI-IMS Analysis. Imaging MS was performed on a MALDI TOF/TOF UltrafleXtreme mass spectrometer equipped with SmartBeam II Nd:YAG/355 nm laser operating at 1 kHz providing a laser spot diameter down to ∼10 μm for the "minimum" focus setting (Bruker Daltonics). Measuring the absolute laser pulse energy of a smartbeam II laser is challenging in UltrafleXtreme systems, as such a measurement would require a reference measurement inside the instrument, which would require modification of the instrument hardware. Moreover, SmartBeam lasers do not have a flat-top shaped beam energy profile, but a rather highly structured beam energy profile, which makes it a hard task to measure the exact value of laser fluence at a flat target surface.[28] Therefore, rather than measuring the laser pulse energy, we provide detailed information about the laser pulse energy settings as previously indicated for lipid analysis in our previous communication; global laser attenuator setting was kept stable at 10% throughout all the experiments and the laser focus set to minimum. Attenuator offset and attenuator range settings were 40% and 10%, respectively, for the minimum laser focus.[20] As SmartBeam II lasers lose some energy output over the lifetime, it is necessary to specify the laser shot count of the instrument unit used for this experimentation, which was about 225696k (∼12 months age).

For dual polarity lipid analysis, profiling and imaging data acquisitions were performed in reflective ion mode under optimized delayed extraction conditions over a mass range of 300−2000 Da. First, IMS data were acquired with five laser shots/per pixel point with a source accelerating voltage of 20 kV in negative polarity (reflector negative mode, RN). This was followed by 50 laser shots/pixel point in positive polarity (reflector positive mode, RP) with a source accelerating voltage of 25 kV. The detector gain value was kept stable at 2626 V for both ionization modes.[20] A mass resolution of $M/\Delta M$ 20 000 was achieved in the mass window of lipids (i.e., 650−1000 Da). External calibration was carried out using peptide calibration standard I (Bruker Daltonics). Image data were reconstructed and root-mean-square (RMS) normalized to minimize pixel to pixel variations of signal intensities (Supporting Information Figure S-8) and visualized using Flex Imaging v3.0 (Bruker Daltonics). Lipid classifications on control tissues were determined by comparing mass accuracy data with the LIPID MAPS database (www.lipidmaps.org) and previous results obtained on mouse brain tissue sections.[5,20,38]

For protein analysis on the same imaging region, the global laser attenuator was increased to 35% while keeping attenuator offset and range settings the same for minimum laser focus. Profiling and imaging data acquisitions were performed in linear positive ion mode in a mass range of 2000−20 000 Da. A number of 50 laser shots/raster spot were acquired with 1 kHz repetition rate. Protein identifications were determined by comparing the mass accuracy data with values reported in the literature[31]

Further, identification of lipids and Aβ1−40 (m/z 4257.6) was achieved by examining MS/MS spectra obtained in LIFT-TOF/TOF mode. MALDI-LIFT (MS/MS) spectra were collected directly in situ in LIFT mode with increased laser power (30%) until a satisfactory intensity of fragment peaks were achieved. (Figure 7 and Supporting Information Figure S-5 and S-6)

Data Analysis. Prior to data analysis, all spectra were calibrated externally using the batch-processing function in Flex Analysis (v 3.0,

DOI: 10.1021/acschemneuro.7b00314
ACS Chem. Neurosci. 2017, 8, 2778−2790

Bruker Daltonics). Calibration spectra were obtained from calibrant solution spots (Protein Calibration Mix 1, Bruker Daltonics) that were placed adjacent to the tissue slides. For the evaluation of dual polarity lipid analysis on the same pixel points, MALDI-IMS data from five replicates of equal pixel-point (80) regions were acquired. Here, cerebellar regions containing equally sized areas of anatomically different cerebellar regions (molecular layer, granular layer, white matter) were analyzed to account for their chemical diversity and distinct stiffness.[66] The laser power was kept constant and the number of laser shots in negative ion mode has been changed to 5, 10, 20, 30, 50, 100 on different regions. Then, positive ion spectra have been collected on the same pixel points along with an equivalent nonirradiated area with a constant number of laser shots (50) as previously optimized for best spectral quality at the laser pulse energy described in MALDI-IMS analysis part.[20] Determination of the intensity of all discernible matrix derived peaks (300−650 Da) and lipid peaks in both ion polarities (300−2000 Da, excluding all matrix peaks) with $S/N \geq 3$ were determined using Flex Analysis 3.0 software. The signal-to-noise calculation is using the intensity as the "signal". The noise calculation is a m/z dependent standard deviation calculation that is done iteratively to remove the data points of peaks which are considered as outliers on top of a background determining the noise. The standard deviation was calculated using five replicates, and the graphs were sketched with Igor Pro 6.3 (Wavemetrics, Lake Oswego, OR).

Image Processing. Image registrations were performed in MATLAB using three consecutive scripts developed in-house using the implemented Image Processing Toolbox. Briefly, the scripts contain cropping images exported from Flex Imaging 3.0, application of transformations for image registration, and resizing/merging the processed images. Brief explanations of the image processing toolbox functions were provided above the scripts as comments. (Supporting Information)

Post-MALDI-IMS H&E Staining. For H&E staining after trimodal MALDI-IMS, the matrix was washed away using 2 × 1 min submersions in 100% EtOH. The tissue was rehydrated in 70% EtOH, 50% EtOH, and Milli-Q water for 2 min each. The slides were placed in hematoxylin (HistoLab Products, Västra Frölunda, Sweden) for 2 min and washed with Milli-Q water for 2 min. The slides were then counterstained in 0.2% eosin (HistoLab Products) for 2 min and washed in Milli-Q water for another 2 min. The section was finally washed and dehydrated in 50% EtOH, 70% EtOH, and 100% EtOH for 1 min each. The tissue sections were mounted with mounting medium (Permount, eBioscience, Thermo Fisher Scientific) and microscopic images were acquired using a wide-field microscope (Zeiss Axio Observer Z1, Zeiss, Jena, Germany).

Immunohistochemistry. Following MALDI IMS analysis of lipids in negative mode, the tissue sections were rinsed in absolute EtOH for 120 s, fixed in 95% EtOH/5% AcOH at −20 °C for 8 min, 70% EtOH at −20 °C for 30 s, 70% EtOH at RT for 30 s, and then stored in PBS prior to antibody staining. Here, a monoclonal antibody specific for the Aβ1−16 epitope (6E10, 1 mg/mL, BioLegend, San Diego, CA) was used as primary antibody, and goat anti-mouse IgG conjugated to FITC 488 (Thermo Fisher Scientific) was used as secondary antibody. The tissue was blocked for 1 h at room temperature (RT) in PBS based blocking solution containing 5% normal goat serum (NGS, Invitrogen, Thermo Fisher Scientific, Carlsbad, CA), 2% bovine serum albumin (BSA, Sigma-Aldrich), and 0.3% Triton-X100 (TX100, Sigma-Aldrich). Incubation with primary antibody (1:500) was performed overnight at 4 °C, and with secondary antibody (1:1000) for 1 h at RT, both diluted in PBS based diluent solution (0.05% NGS, 0.02% BSA, 0.3% TX100). Unspecific binding of the secondary antibody was assessed by incubation of in diluent solution without the primary antibody. Each incubation step was followed by 3 × 5 min rinse in PBS. Prior to imaging tissue was mounted with Prolong Gold antifade reagent (Thermo Fisher Scientific) and dried for 2 h at RT. Imaging was performed using a wide field microscope (Axio Observer Z1, Zeiss, Jena, Germany).

■ ASSOCIATED CONTENT

Supporting Information

The Supporting Information is available free of charge on the ACS Publications website at DOI: 10.1021/acschemneuro.7b00314.

IMS3 protocol optimization; H&E staining following IMS3; immunohistochemistry of amyloid plaques; control IMS on WT mouse tissue; MS/MS data for lipid and peptide identification; MS data for evaluating the effect of matrix deposition amount on spectral quality; control IMS data for illustrating normalization effects; Matlab script for image processing (PDF)

■ AUTHOR INFORMATION

Corresponding Author

*Mailing address: Department of Psychiatry and Neurochemistry, Sahlgrenska Academy at the University of Gothenburg, Mölndal Hospital, House V, Biskopsbogatan 27, SE-43180 Mölndal, Sweden. E-mail: jh@gu.se. Tel: +46-31-343 23 77.

ORCID

Jörg Hanrieder: 0000-0001-6059-198X

Author Contributions

J.H. and I.K. conceived and designed the study. I.K. designed and performed all MALDI experiments. I.K and D.B developed and optimized sample preparation for high-resolution protein MALDI-IMS. W.M. performed H&E and IHC staining experiments. M.B. wrote the MATLAB script for image coregistration. I.K. and J.H. analyzed the data and drafted the manuscript. I.K., D.B., H.Z., K.B., and J.H. discussed the data and wrote the manuscript. All the authors approved the final version of the manuscript.

Funding

The Swedish Research Council VR (no. 2014-6447, J.H.; no. 2012-1593, H.Z.; no. 2012-2288, K.B.), the Royal Society of Arts and Sciences in Gothenburg (KVVS, J.H.), Alzheimerfonden (J.H., K.B.), Demensfonden (J.H.), Hjärnfonden (K.B.), Jeanssons Stiftelsen (J.H.), Ahlén Stiftelsen (J.H.), Stiftelsen Gamla Tjänarinnor (J.H., K.B., W.M.), Stohnes Stiftelse (J.H.), the Torsten Söderberg Foundation (K.B.), and Stiftelsen Wilhelm och Martina Lundgrens Vetenskapsfond (J.H.) are acknowledged for financial support.

Notes

The authors declare no competing financial interest.

■ ACKNOWLEDGMENTS

We thank Dr. Stina Syvänen and Dr. Dag Sehlin at Uppsala University for providing the tgArcSwe mouse brain samples. The work was in part performed at the go:IMS imaging MS infrastructure at the University of Gothenburg (www.go-ims.gu.se) headed by Prof. Andrew Ewing. We thank the staff at Centre for Cellular Imaging (CCI), Core Facilities, The Sahlgrenska Academy, University of Gothenburg, Gothenburg, Sweden.

■ LIST OF ABBREVIATIONS

AD, Alzheimer's disease; Aβ, amyloid beta; Cer, ceramides; FA, formic acid; IHC, immunohistochemistry; IMS, imaging mass spectrometry; ITO, indium tin-oxide; LPC, lysophosphatidylcholine; MALDI, matrix-assisted laser desorption/ionization; OCT, optimal cutting temperature; PC, phosphatidylcholine;

DOI: 10.1021/acschemneuro.7b00314
ACS Chem. Neurosci. 2017, 8, 2778−2790

PE, phosphatidylethanolamine; PI, phosphatidylinositols; PG, phosphatidylglycerol; PS, phosphatidylserine; RN, reflector negative mode; RMS, root-mean-square; ROI, region of interest; RP, reflector positive mode; SM, sphingomyelin; ST, sulfatides; TOF, time-of-flight.

REFERENCES

(1) Cornett, D. S., Frappier, S. L., and Caprioli, R. M. (2008) MALDI-FTICR imaging mass spectrometry of drugs and metabolites in tissue. *Anal. Chem. 80*, 5648−5653.

(2) Caprioli, R. M., Farmer, T. B., and Gile, J. (1997) Molecular imaging of biological samples: localization of peptides and proteins using MALDI-TOF MS. *Anal. Chem. 69*, 4751−4760.

(3) Chaurand, P., Stoeckli, M., and Caprioli, R. M. (1999) Direct profiling of proteins in biological tissue sections by MALDI mass spectrometry. *Anal. Chem. 71*, 5263−5270.

(4) Chaurand, P., Cornett, D. S., Angel, P. M., and Caprioli, R. M. (2011) From whole-body sections down to cellular level, multiscale imaging of phospholipids by MALDI mass spectrometry. *Mol. Cell. Proteomics 10*, 004259.

(5) Thomas, A. l., Charbonneau, J. L., Fournaise, E., and Chaurand, P. (2012) Sublimation of new matrix candidates for high spatial resolution imaging mass spectrometry of lipids: enhanced information in both positive and negative polarities after 1, 5-diaminonapthalene deposition. *Anal. Chem. 84*, 2048−2054.

(6) Hanrieder, J., Phan, N. T. N., Kurczy, M. E., and Ewing, A. G. (2013) Imaging Mass Spectrometry in Neuroscience. *ACS Chem. Neurosci. 4*, 666−679.

(7) Tanaka, K., Waki, H., Ido, Y., Akita, S., Yoshida, Y., Yoshida, T., and Matsuo, T. (1988) Protein and polymer analyses up to m/z 100 000 by laser ionization time? of? flight mass spectrometry. *Rapid Commun. Mass Spectrom. 2*, 151−153.

(8) Karas, M., and Hillenkamp, F. (1988) Laser desorption ionization of proteins with molecular masses exceeding 10,000 Da. *Anal. Chem. 60*, 2299−2301.

(9) Karas, M., and Krüger, R. (2003) Ion formation in MALDI: the cluster ionization mechanism. *Chem. Rev. 103*, 427−440.

(10) Knochenmuss, R. (2006) Ion formation mechanisms in UV-MALDI. *Analyst 131*, 966−986.

(11) Dreisewerd, K. (2003) The desorption process in MALDI,. *Chem. Rev. 103*, 395−426.

(12) Karas, M., Glückmann, M., and Schäfer, J. (2000) Ionization in matrix-assisted laser desorption/ionization: singly charged molecular ions are the lucky survivors. *J. Mass Spectrom. 35*, 1−12.

(13) Soltwisch, J., Jaskolla, T. W., Hillenkamp, F., Karas, M., and Dreisewerd, K. (2012) Ion yields in UV-MALDI mass spectrometry as a function of excitation laser wavelength and optical and physico-chemical properties of classical and halogen-substituted MALDI matrixes. *Anal. Chem. 84*, 6567−6576.

(14) Horneffer, V., Dreisewerd, K., Lüdemann, H.-C., Hillenkamp, F., Läge, M., and Strupat, K. (1999) Is the incorporation of analytes into matrix crystals a prerequisite for matrix-assisted laser desorption/ionization mass spectrometry? A study of five positional isomers of dihydroxybenzoic acid,. *Int. J. Mass Spectrom. 185*, 859−870.

(15) Jaskolla, T. W., and Karas, M. (2011) Compelling evidence for lucky survivor and gas phase protonation: the unified MALDI analyte protonation mechanism. *J. Am. Soc. Mass Spectrom. 22*, 976−988.

(16) Garrett, T. J., Prieto-Conaway, M. C., Kovtoun, V., Bui, H., Izgarian, N., Stafford, G., and Yost, R. A. (2007) Imaging of small molecules in tissue sections with a new intermediate-pressure MALDI linear ion trap mass spectrometer. *Int. J. Mass Spectrom. 260*, 166−176.

(17) Steven, R. T., and Bunch, J. (2013) Repeat MALDI MS imaging of a single tissue section using multiple matrices and tissue washes. *Anal. Bioanal. Chem. 405*, 4719−4728.

(18) Molin, L., Seraglia, R., Dani, F. R., Moneti, G., and Traldi, P. (2011) The double nature of 1, 5-diaminonaphthalene as matrix-assisted laser desorption/ionization matrix: some experimental evidence of the protonation and reduction mechanisms,. *Rapid Commun. Mass Spectrom. 25*, 3091−3096.

(19) Ellis, S. R., Cappell, J., Potočnik, N. O., Balluff, B., Hamaide, J., Van der Linden, A., and Heeren, R. M. (2016) More from less: high-throughput dual polarity lipid imaging of biological tissues. *Analyst 141*, 3832.

(20) Kaya, I., Michno, W., Brinet, D., Iacone, Y., Zanni, G., Blennow, K., Zetterberg, H., and Hanrieder, J. r. (2017) Histology-Compatible MALDI Mass Spectrometry Based Imaging of Neuronal Lipids for Subsequent Immunofluorescent Staining. *Anal. Chem. 89*, 4685−4694.

(21) Hankin, J. A., Barkley, R. M., and Murphy, R. C. (2007) Sublimation as a method of matrix application for mass spectrometric imaging. *J. Am. Soc. Mass Spectrom. 18*, 1646−1652.

(22) Zemski Berry, K. A., Hankin, J. A., Barkley, R. M., Spraggins, J. M., Caprioli, R. M., and Murphy, R. C. (2011) MALDI imaging of lipid biochemistry in tissues by mass spectrometry. *Chem. Rev. 111*, 6491−6512.

(23) Ogrinc Potočnik, N., Porta, T., Becker, M., Heeren, R., and Ellis, S. R. (2015) Use of advantageous, volatile matrices enabled by next-generation high-speed matrix-assisted laser desorption/ionization time-of-flight imaging employing a scanning laser beam. *Rapid Commun. Mass Spectrom. 29*, 2195−2203.

(24) Jaskolla, T. W., Karas, M., Roth, U., Steinert, K., Menzel, C., and Reihs, K. (2009) Comparison between vacuum sublimed matrices and conventional dried droplet preparation in MALDI-TOF mass spectrometry. *J. Am. Soc. Mass Spectrom. 20*, 1104−1114.

(25) Mao, X., Chan, W.-T., Caetano, M., Shannon, M. A., and Russo, R. E. (1996) Preferential vaporization and plasma shielding during nano-second laser ablation. *Appl. Surf. Sci. 96*, 126−130.

(26) Vogel, A., and Venugopalan, V. (2003) Mechanisms of pulsed laser ablation of biological tissues. *Chem. Rev. 103*, 577−644.

(27) Fournier, I., Marinach, C., Tabet, J., and Bolbach, G. (2003) Irradiation effects in MALDI, ablation, ion production, and surface modifications. Part II: 2, 5-dihydroxybenzoic acid monocrystals. *J. Am. Soc. Mass Spectrom. 14*, 893−899.

(28) Holle, A., Haase, A., Kayser, M., and Hohndorf, J. (2006) Optimizing UV laser focus profiles for improved MALDI performance Holle, Armin; Haase, Andreas; Kayser, Markus; Hoehndorf. *J. Mass Spectrom. 41*, 705−716.

(29) Wenzel, T., Sparbier, K., Mieruch, T., and Kostrzewa, M. (2006) 2, 5-Dihydroxyacetophenone: a matrix for highly sensitive matrix-assisted laser desorption/ionization time-of-flight mass spectrometric analysis of proteins using manual and automated preparation techniques. *Rapid Commun. Mass Spectrom. 20*, 785−789.

(30) Zavalin, A., Yang, J., Hayden, K., Vestal, M., and Caprioli, R. M. (2015) Tissue protein imaging at 1 μm laser spot diameter for high spatial resolution and high imaging speed using transmission geometry MALDI TOF MS. *Anal. Bioanal. Chem. 407*, 2337−2342.

(31) Hanrieder, J., Malmberg, P., and Ewing, A. G. (2015) Spatial neuroproteomics using imaging mass spectrometry. *Biochim. Biophys. Acta, Proteins Proteomics 1854*, 718−731.

(32) Ross, C. A., and Poirier, M. A. (2004) Protein aggregation and neurodegenerative disease. *Nat. Med. 10*, S10.

(33) Selkoe, D. J. (2002) Alzheimer's disease is a synaptic failure. *Science 298*, 789−791.

(34) Hardy, J., and Selkoe, D. J. (2002) The amyloid hypothesis of Alzheimer's disease: progress and problems on the road to therapeutics,. *Science 297*, 353−356.

(35) Ahmed, M., Davis, J., Aucoin, D., Sato, T., Ahuja, S., Aimoto, S., Elliott, J. I., Van Nostrand, W. E., and Smith, S. O. (2010) Structural conversion of neurotoxic amyloid-[beta] 1−42 oligomers to fibrils. *Nat. Struct. Mol. Biol. 17*, 561−567.

(36) Refolo, L. M., Pappolla, M. A., Malester, B., LaFrancois, J., Bryant-Thomas, T., Wang, R., Tint, G. S., Sambamurti, K., and Duff, K. (2000) Hypercholesterolemia accelerates the Alzheimer's amyloid pathology in a transgenic mouse model. *Neurobiol. Dis. 7*, 321−331.

(37) Cutler, R. G., Kelly, J., Storie, K., Pedersen, W. A., Tammara, A., Hatanpaa, K., Troncoso, J. C., and Mattson, M. P. (2004) Involvement of oxidative stress-induced abnormalities in ceramide and cholesterol

DOI: 10.1021/acschemneuro.7b00314
ACS Chem. Neurosci. 2017, 8, 2778−2790

metabolism in brain aging and Alzheimer's disease. *Proc. Natl. Acad. Sci. 101*, 2070−2075.
(38) Kaya, I., Brinet, D., Michno, W., Syvänen, S., Sehlin, D., Zetterberg, H., Blennow, K., and Hanrieder, J. r. (2017) Delineating Amyloid Plaque Associated Neuronal Sphingolipids in Transgenic Alzheimer's Disease Mice (tgArcSwe) Using MALDI Imaging Mass Spectrometry. *ACS Chem. Neurosci. 8*, 347−355.
(39) Yanagisawa, K., Odaka, A., Suzuki, N., and Ihara, Y. (1995) GM1 ganglioside−bound amyloid β−protein (Aβ): A possible form of preamyloid in Alzheimer's disease,. *Nat. Med. 1*, 1062−1066.
(40) Chan, R. B., Oliveira, T. G., Cortes, E. P., Honig, L. S., Duff, K. E., Small, S. A., Wenk, M. R., Shui, G., and Di Paolo, G. (2012) Comparative lipidomic analysis of mouse and human brain with Alzheimer disease. *J. Biol. Chem. 287*, 2678−2688.
(41) Hong, J. H., Kang, J. W., Kim, D. K., Baik, S. H., Kim, K. H., Shanta, S. R., Jung, J. H., Mook-Jung, I., and Kim, K. P. (2016) Global changes of phospholipids identified by MALDI imaging mass spectrometry in a mouse model of Alzheimer's disease. *J. Lipid Res. 57*, 36−45.
(42) Sheikh, A. M., Michikawa, M., Kim, S., and Nagai, A. (2015) Lysophosphatidylcholine increases the neurotoxicity of Alzheimer's amyloid β 1−42 peptide: Role of oligomer formation. *Neuroscience 292*, 159−169.
(43) Di Paolo, G., and Kim, T.-W. (2011) Linking lipids to Alzheimer's disease: cholesterol and beyond. *Nat. Rev. Neurosci. 12*, 284−296.
(44) Carlred, L., Michno, W., Kaya, I., Sjövall, P., Syvänen, S., and Hanrieder, J. (2016) Probing Amyloid-β Pathology in transgenic Alzheimer's disease (tgArcSwe) mice using MALDI Imaging Mass Spectrometry. *J. Neurochem. 138*, 469.
(45) Lord, A., Kalimo, H., Eckman, C., Zhang, X.-Q., Lannfelt, L., and Nilsson, L. N. (2006) The Arctic Alzheimer mutation facilitates early intraneuronal Aβ aggregation and senile plaque formation in transgenic mice,. *Neurobiol. Aging 27*, 67−77.
(46) Han, X. M., Holtzman, D. W., McKeel, D., Kelley, J., and Morris, J. C. (2002) Substantial sulfatide deficiency and ceramide elevation in very early Alzheimer's disease: potential role in disease pathogenesis. *J. Neurochem. 82*, 809−818.
(47) Hirahara, Y., Wakabayashi, T., Mori, T., Koike, T., Yao, I., Tsuda, M., Honke, K., Gotoh, H., Ono, K., and Yamada, H. (2017) Sulfatide species with various fatty acid chains in oligodendrocytes at different developmental stages determined by imaging mass spectrometry. *J. Neurochem. 140*, 435−450.
(48) Cheng, H., Zhou, Y., Holtzman, D. M., and Han, X. (2010) Apolipoprotein E mediates sulfatide depletion in animal models of Alzheimer's disease. *Neurobiol. Aging 31*, 1188−1196.
(49) Han, X. (2007) Potential mechanisms contributing to sulfatide depletion at the earliest clinically recognizable stage of Alzheimer's disease: a tale of shotgun lipidomics. *J. Neurochem. 103*, 171−179.
(50) Back, S. A., Gan, X., Li, Y., Rosenberg, P. A., and Volpe, J. J. (1998) Maturation-dependent vulnerability of oligodendrocytes to oxidative stress-induced death caused by glutathione depletion. *J. Neurosci. 18*, 6241−6253.
(51) Al-Mashhadi, S., Simpson, J. E., Heath, P. R., Dickman, M., Forster, G., Matthews, F. E., Brayne, C., Ince, P. G., and Wharton, S. B. (2015) Oxidative glial cell damage associated with white matter lesions in the aging human brain. *Brain Pathol. 25*, 565−574.
(52) Mitew, S., Kirkcaldie, M. T., Halliday, G. M., Shepherd, C. E., Vickers, J. C., and Dickson, T. C. (2010) Focal demyelination in Alzheimer's disease and transgenic mouse models. *Acta Neuropathol. 119*, 567−577.
(53) Sanchez-Mejia, R. O., Newman, J. W., Toh, S., Yu, G.-Q., Zhou, Y., Halabisky, B., Cissé, M., Scearce-Levie, K., Cheng, I. H., Gan, L., et al. (2008) Phospholipase A2 reduction ameliorates cognitive deficits in a mouse model of Alzheimer's disease. *Nat. Neurosci. 11*, 1311−1318.
(54) Berman, D. E., Dall'Armi, C., Voronov, S. V., McIntire, L. B. J., Zhang, H., Moore, A. Z., Staniszewski, A., Arancio, O., Kim, T.-W., and Di Paolo, G. (2008) Oligomeric amyloid-β peptide disrupts phosphatidylinositol-4, 5-bisphosphate metabolism. *Nat. Neurosci. 11*, 547−554.
(55) Sundaram, J. R., Chan, E. S., Poore, C. P., Pareek, T. K., Cheong, W. F., Shui, G., Tang, N., Low, C.-M., Wenk, M. R., and Kesavapany, S. (2012) Cdk5/p25-induced cytosolic PLA2-mediated lysophosphatidylcholine production regulates neuroinflammation and triggers neurodegeneration. *J. Neurosci. 32*, 1020−1034.
(56) Sheikh, A. M., and Nagai, A. (2011) Lysophosphatidylcholine modulates fibril formation of amyloid beta peptide. *FEBS J. 278*, 634−642.
(57) Allt, G., Ghabriel, M., and Sikri, K. (1988) Lysophosphatidyl choline-induced demyelination. *Acta Neuropathol. 75*, 456−464.
(58) Nitsch, R. M., Blusztajn, J. K., Pittas, A. G., Slack, B. E., Growdon, J. H., and Wurtman, R. J. (1992) Evidence for a membrane defect in Alzheimer disease brain. *Proc. Natl. Acad. Sci. 89*, 1671−1675.
(59) Prasad, M. R., Lovell, M. A., Yatin, M., Dhillon, H., and Markesbery, W. R. (1998) Regional membrane phospholipid alterations in Alzheimer's disease. *Neurochem. Res. 23*, 81−88.
(60) McLaurin, J., Franklin, T., Chakrabartty, A., and Fraser, P. (1998) Phosphatidylinositol and inositol involvement in Alzheimer amyloid-β fibril growth and arrest. *J. Mol. Biol. 278*, 183−194.
(61) Jolles, J., Bothmer, J., Markerink, M., and Ravid, R. (1992) Phosphatidylinositol kinase is reduced in Alzheimer's disease. *J. Neurochem. 58*, 2326−2329.
(62) Biemann, K. (1990) Sequencing of peptides by tandem mass spectrometry and high-energy collision-induced dissociation. *Methods Enzymol. 193*, 455−479.
(63) Kaufmann, R., Kirsch, D., and Spengler, B. (1994) Sequenching of peptides in a time-of-flight mass spectrometer: evaluation of postsource decay following matrix-assisted laser desorption ionisation (MALDI). *Int. J. Mass Spectrom. Ion Processes 131*, 355−385.
(64) Brown, R. S., and Lennon, J. J. (1995) Sequence-specific fragmentation of matrix-assisted laser-desorbed protein/peptide ions. *Anal. Chem. 67*, 3990−3999.
(65) Yang, J., and Caprioli, R. M. (2011) Matrix sublimation/recrystallization for imaging proteins by mass spectrometry at high spatial resolution. *Anal. Chem. 83*, 5728−5734.
(66) Weickenmeier, J., de Rooij, R., Budday, S., Steinmann, P., Ovaert, T., and Kuhl, E. (2016) Brain stiffness increases with myelin content. *Acta Biomater. 42*, 265−272.

DOI: 10.1021/acschemneuro.7b00314
ACS Chem. Neurosci. 2017, 8, 2778−2790